Research Article

Theoretical Analysis of Cu-H$_2$O, Al$_2$O$_3$-H$_2$O, and TiO$_2$-H$_2$O Nanofluid Flow Past a Rotating Disk with Velocity Slip and Convective Conditions

Abdullah Dawar,[1] Ebenezer Bonyah [iD],[2] Saeed Islam [iD],[1] Ahmed Alshehri,[3] and Zahir Shah[4]

[1]Department of Mathematics, Abdul Wali Khan University, Mardan, Mardan, 23200 Khyber Pakhtunkhwa, Pakistan
[2]Department of Mathematics Education, University of Education Winnebakumasi-(Kumasicompus), Kumasi 00233, Ghana
[3]Department of Mathematics, Faculty of Sciences, King Abdulaziz University, Jeddah 21589, Saudi Arabia
[4]Department of Mathematical Sciences, University of Lakki Marwat, Lakki Marwat, 28420 Khyber Pakhtunkhwa, Pakistan

Correspondence should be addressed to Ebenezer Bonyah; ebbonya@gmail.com

The nanofluids can be used in the subsequent precise areas like chemical nanofluids, environmental nanofluids, heat transfer nanofluids, pharmaceutical nanofluids, drug delivery nanofluids, and process/extraction nanofluids. In short, the number of engineering and industrial applications of nanofluid technologies, as well as their emphasis on particular industrial applications, has been increased recently. Therefore, this exploration is carried out to analyze the nanofluid flow past a rotating disk with velocity slip and convective conditions. The water-based spherical-shaped nanoparticles of copper, alumina, and titanium have been considered in this analysis. The modeled problem has been solved with the help of homotopic technique. Convergence of the homotopic technique is shown with the help of the figure. The role of the physical factors on radial and tangential velocities, temperature, surface drag force, and heat transfer rate are displayed through figures and tables. The outcomes demonstrate that the surface drag force of the water-based spherical-shaped nanoparticles of Cu, Al$_2$O$_3$, and TiO$_2$ has been reduced with a greater magnetic field. The radial and tangential velocities of the water-based spherical-shaped nanoparticles of Cu, Al$_2$O$_3$, and TiO$_2$, and pure water have been augmented via magnetic parameter. The radial velocity of the water-based spherical-shaped nanoparticle of Cu has been augmented via nanoparticle volume fraction, whereas reduced for the Al$_2$O$_3$ and TiO$_2$ nanoparticles. The tangential velocity of the water-based spherical-shaped nanoparticles of Cu, Al$_2$O$_3$, and TiO$_2$ has reduced via nanoparticle volume fraction. Also, the variations in radial and tangential velocities are greater for slip conditions as compared to no-slip conditions.

1. Introduction

The suspension of nanosized (between 1 nm and 100 nm) material into conventional fluids such as oil, ethylene glycol, water, and sodium alginate is called nanofluids. Nanofluids with their innovative and advanced ideas have intriguing thermal transfer properties as opposed to traditional heat transfer fluids. There has been a great deal of research into nanofluids' dominant heat transfer properties, especially convective heat transfer and thermal conductivity. With these properties, nanofluid implementations in industries like heat exchange systems look promising. The nanofluids can be used in the subsequent precise areas like chemical nanofluids, environmental nanofluids, heat transfer nanofluids, pharmaceutical nanofluids, drug delivery nanofluids, and process/extraction nanofluids. In short, the number of engineering and industrial applications of nanofluids technologies, as well as their emphasis on particular industrial applications, has been increased recently [1–7]. The capability of thermal transmission of nanofluids can be quantified by their properties like specific heat, density, viscosity, and thermal conductivity. The thermal properties are contingent on the shape, base fluid,

particle size, material, and concentration. To utilize the applications towards engineering and industries, researchers are working on the evaluation and characterization of the thermophysical properties of nanofluids for heat transfer analysis [8]. Sheikholeslami [9] analyzed the different shapes of aluminum oxide using the Darcy porous medium with thermal radiation. Hayat et al. [10] investigated the nanofluid flow with Hall and Ohmic influences. They deliberated the thermal convective and velocity slip boundary conditions. The Hall and Ohmic parameters have reduced the velocity and heat transfer rate. Sheikholeslami [11] presented the analysis different shapes of nanoparticles of copper oxide water with Brownian motion. It has been introduced that the platelet shape nanoparticles has leading impression as associated to other shapes of nanoparticles. Thumma et al. [12] investigated the non-Newtonian nanofluid flow containing water-based CuO and Cu nanoparticles past porous extending sheet with entropy optimization and velocity condition. A non-Fourier has been implemented to analyze the heat transfer rate. Hayat et al. [13] examined the Cu, Fe_2O_3, and Au nanoparticles with Hall and Ohmic effects using constant and variable viscosities. Sheikholeslami et al. [14] addressed the Al_2O_3-water nanoparticles through a channel with Brownian motion impact. Thumma et al. [15] deliberated the radiative boundary layer nanofluid flow past a nonlinear extending surface with viscous dissipation. Rout et al. [16] analyzed the water-based Cu and kerosene oil-based Cu between two parallel plates with thermal radiation. Further studies related to nanofluids are mentioned in [17–26].

The flow behavior of a flowing conducting liquid is described by magnetohydrodynamic (MHD), which polarizes it. In industrial activities such as nuclear power plants, crystal manufacture, electric generators, and fuel industry, the impact of magnetic fields is assessed. Tamim et al. [27] addressed the MHD mixed convective flow of nanofluid on a vertical plate. They studied both opposing and assisting flows. The water-based Cu, Al_2O_3, and TiO_2 are examined. Ghadikolaei et al. [28] implemented the induced magnetic field on hybrid nanofluid flow through an extending surface. Hayat et al. [29] explore the unsteady MHD viscous fluid flow with Joule heating, thermal radiation, and thermal stratification influences. Ahmad et al. [30] expressed the MHD flow of ferrofluid past an exponentially extending surface. Singh et al. [31] investigated the MHD flow of water-based alumina nanofluid past a flat plate with slip condition. Mliki et al. [32] evaluated the convective nanofluid flow with MHD effect. Upreti et al. [33] presented the CNT nanofluids past an extending surface with nonuniform heat source/sink and Ohmic heating. Pandey et al. [34] presented the MHD water-based copper nanofluid flow inside a convergent/divergent channel. Upreti et al. examined the MHD Ag-kerosene oil nanofluid with suction/injection roles. Turkyilmazoglu [35] presented the viscous fluid flow with magnetic field impact past a spinning disk. The MHD viscous fluid flow considering wall slip conditions has been investigated by Hussain et al. [36]. Dawar et al. [19] presented the highly magnetized and nonmagnetized non-Newtonian fluid flow past an extending cylinder. Further related results can be seen in [18, 37–45].

Magnetic nanoparticles pique the researchers' interest in various fields, including homogeneous and heterogeneous catalysis, magnetic fluids, environmental remediation, biomedicine, data storage, and magnetic resonance imaging (MRI) for instance purification of water. The literature proves that the nanoparticles of size less than the critical value (i.e., 10-20 nm) perform best [46]. Nanoparticles' magnetic properties effectively monopolize at such a small scale, rendering them beneficial and helpful in a wide range of applications [46–49]. In light of the abovementioned applications, we have considered a mathematical model for the flow of nanofluid containing the nanoparticles of Cu-H_2O, Al_2O_3-H_2O, and TiO_2-H_2O, and pure water with a strong magnetic field. According to the authors knowledge, there is no study based on spherical-shaped nanoparticles of the Cu, Al_2O_3, and TiO_2 using water as a based fluid past a rotating disk. Furthermore, the velocity slip and convective conditions are considered to analyze the flow behavior in the presence and absence of slip conditions. The mathematical model is solved with the help of the homotopic approach.

2. Physical Model

We consider the water-based nanomaterials (Cu, Al_2O_3, and TiO_2) past a rotating disk. The velocity components $\tilde{u}_1, \tilde{u}_2$, and $\tilde{u}_3$ are taken along $\tilde{r}, \phi$, and $\tilde{z}$ directions, respectively. The disk rotates with an angular velocity Ω at $\tilde{z} = 0$ (see Figure 1). A magnetic field of strength B_0 is applied normal to the fluid flow. The flow is subjected to velocity slip and thermal convective conditions. The leading equations are defined as follows [35]:

$$\frac{\partial \tilde{u}_1}{\partial \tilde{r}} + \frac{\tilde{u}_1}{\tilde{r}} + \frac{\partial \tilde{u}_3}{\partial \tilde{z}} = 0,$$

$$\tilde{u}_1 \frac{\partial \tilde{u}_1}{\partial r} - \frac{\tilde{u}_2^2}{r} + \tilde{u}_3 \frac{\partial \tilde{u}_1}{\partial z} = -\frac{1}{\rho_{nf}} \frac{\partial \tilde{p}}{\partial \tilde{r}} + \frac{\mu_{nf}}{\rho_{nf}}$$
$$\cdot \left(\frac{\partial^2 \tilde{u}_1}{\partial \tilde{r}^2} + \frac{1}{\tilde{r}} \frac{\partial \tilde{u}_1}{\partial \tilde{r}} - \frac{\tilde{u}_1}{\tilde{r}^2} + \frac{\partial^2 \tilde{u}_1}{\partial \tilde{z}^2} \right)$$
$$- \frac{\sigma_{nf}}{\rho_{nf}} B_0^2 \tilde{u}_1,$$

$$\tilde{u}_1 \frac{\partial \tilde{u}_2}{\partial \tilde{r}} + \frac{\tilde{u}_1 \tilde{u}_2}{\tilde{r}} + \tilde{u}_3 \frac{\partial \tilde{u}_2}{\partial \tilde{z}} = \frac{\mu_{nf}}{\rho_{nf}} \left(\frac{\partial^2 \tilde{u}_2}{\partial \tilde{r}^2} + \frac{1}{\tilde{r}} \frac{\partial \tilde{u}_2}{\partial \tilde{r}} - \frac{\tilde{u}_2}{\tilde{r}^2} + \frac{\partial^2 \tilde{u}_2}{\partial \tilde{z}^2} \right)$$
$$- \frac{\sigma_{nf}}{\rho_{nf}} B_0^2 \tilde{u}_2,$$

$$\tilde{u}_1 \frac{\partial \tilde{u}_3}{\partial \tilde{r}} + \tilde{u}_3 \frac{\partial \tilde{u}_3}{\partial \tilde{z}} = -\frac{1}{\rho_{nf}} \frac{\partial \tilde{p}}{\partial \tilde{z}} + \frac{\mu_{nf}}{\rho_{nf}} \left(\frac{\partial^2 \tilde{u}_3}{\partial \tilde{r}^2} + \frac{1}{\tilde{r}} \frac{\partial \tilde{u}_3}{\partial \tilde{r}} + \frac{\partial^2 \tilde{u}_3}{\partial \tilde{z}^2} \right),$$

$$\tilde{u}_1 \frac{\partial \tilde{T}}{\partial \tilde{r}} + \tilde{u}_3 \frac{\partial \tilde{T}}{\partial \tilde{z}} = \frac{k_{nf}}{(\rho c_p)_{nf}} \left(\frac{\partial^2 \tilde{T}}{\partial \tilde{r}^2} + \frac{1}{\tilde{r}} \frac{\partial \tilde{T}}{\partial \tilde{r}} + \frac{\partial^2 \tilde{T}}{\partial \tilde{z}^2} \right), \quad (1)$$

with boundary conditions:

$$\left\{ \begin{array}{l} \tilde{u}_1 = L \frac{\partial \tilde{u}_1}{\partial \tilde{z}}, \tilde{u}_2 = L \frac{\partial \tilde{u}_2}{\partial \tilde{z}} + \Omega \cdot \tilde{r}, \tilde{u}_3 = 0, -k_{nf} \frac{\partial \tilde{T}}{\partial \tilde{z}} = h_f \left(\tilde{T}_f - \tilde{T} \right) \text{at } \tilde{z} = 0 \\ \tilde{u}_1 \longrightarrow 0, \tilde{u}_2 \longrightarrow 0, \tilde{T} \longrightarrow \tilde{T}_\infty \text{as } \tilde{z} \longrightarrow \infty \end{array} \right\}.$$
$$(2)$$

The thermophysical properties of the nanofluids are defined as [50]

$$\left\{ \begin{array}{l} \dfrac{\mu_{\mathrm{nf}}}{\mu_{\mathrm{f}}} = \dfrac{1}{(1-\varphi)^{2.5}}, \dfrac{\rho_{\mathrm{nf}}}{\rho_{\mathrm{f}}} = (1-\varphi) + \varphi\dfrac{\rho_{\mathrm{np}}}{\rho_{\mathrm{f}}}, \dfrac{(\rho c_p)_{\mathrm{nf}}}{(\rho c_p)_{\mathrm{f}}} = (1-\varphi) + \varphi\dfrac{(\rho c_p)_{\mathrm{np}}}{(\rho c_p)_{\mathrm{f}}} \\[4mm] \dfrac{\sigma_{\mathrm{nf}}}{\sigma_f} = 1 + \dfrac{3((\sigma_{\mathrm{np}}/\sigma_{\mathrm{f}}) - 1)\varphi}{((\sigma_{\mathrm{np}}/\sigma_{\mathrm{f}}) + 2) - ((\sigma_{\mathrm{np}}/\sigma_{\mathrm{f}}) - 1)\varphi}, \dfrac{k_{\mathrm{nf}}}{k_{\mathrm{f}}} = \dfrac{k_{\mathrm{np}} + (n-1)k_{\mathrm{f}} - (n-1)(k_{\mathrm{f}} - k_{\mathrm{np}})\varphi}{k_{\mathrm{np}} + (n-1)k_{\mathrm{f}} + (k_{\mathrm{f}} - k_{\mathrm{np}})\varphi} \end{array} \right\}. \tag{3}$$

In the above equations, μ is the dynamic viscosity, ρ is the density, c_p is the heat capacitance, L is the wall slip parameter, $\tilde{p}$ is the pressure, k is the thermal conductivity, and φ represents the volume fraction of the nanoparticles. Furthermore, the subscript f indicates the base fluid, nf shows the nanofluids, and np is used for nanoparticles.

The correspondence variables are defined as [53–55]

$$\left\{ \begin{array}{l} \tilde{u}_1 = \tilde{r}\Omega f(\eta), \tilde{u}_2 = \tilde{r}\Omega g(\eta), \tilde{u}_3 = \sqrt{\Omega \nu_{\mathrm{f}}}h(\eta) \\[3mm] \tilde{p} = \tilde{p}_{\infty} + 2\Omega\mu_{\mathrm{f}}\tilde{P}(\eta), \tilde{T} = \tilde{T}_{\infty} + \left(\tilde{T}_{\mathrm{f}} - \tilde{T}_{\infty}\right)\theta(\eta), \eta = \sqrt{\dfrac{\Omega}{\nu_{\mathrm{f}}}}\tilde{z} \end{array} \right\}. \tag{4}$$

The above system is transformed as

$$h' + 2f = 0,$$

$$f'' + \frac{\bar{M}_2}{\bar{M}_1}\left[hf' - f^2 + g^2\right] - \frac{\bar{M}_3}{\bar{M}_1}Mf = 0,$$

$$g'' - \frac{\bar{M}_2}{\bar{M}_1}\left[2gf + g'h\right] - \frac{\bar{M}_3}{\bar{M}_1}Mg = 0, \tag{5}$$

$$\theta'' - \frac{\bar{M}_5}{\bar{M}_4}\Pr\theta'h = 0,$$

where

$$\left\{\bar{M}_1 = \frac{\mu_{\mathrm{nf}}}{\mu_{\mathrm{f}}}, \bar{M}_2 = \frac{\rho_{\mathrm{nf}}}{\rho_{\mathrm{f}}}, \bar{M}_3 = \frac{\sigma_{\mathrm{nf}}}{\sigma_{\mathrm{f}}}, \bar{M}_4 = \frac{k_{\mathrm{nf}}}{k_{\mathrm{f}}}, \bar{M}_5 = \frac{(\rho c_p)_{\mathrm{nf}}}{(\rho c_p)_{\mathrm{f}}}\right\}. \tag{6}$$

with

$$\left\{ \begin{array}{l} f(0) = \alpha f'(0), g(0) = 1 + \alpha g'(0), h(0) = 0, \dfrac{k_{\mathrm{nf}}}{k_{\mathrm{f}}}\theta'(0) = \mathrm{Bi}(\theta(0) - 1) \\[3mm] f(\eta \longrightarrow \infty) \longrightarrow 0, g(\eta \longrightarrow \infty) \longrightarrow 0, \theta(\eta \longrightarrow \infty) \longrightarrow 0 \end{array} \right\}. \tag{7}$$

Here, $M = \sigma_f B_0^2/\rho_f\Omega$ is the magnetic parameter, $\Pr = \nu_{\mathrm{f}}/\alpha_{\mathrm{f}}$ is the Prandtl number, $\alpha = L\tilde{r}\sqrt{\Omega/\nu_{\mathrm{f}}}$ is the wall slip parameter, and $\mathrm{Bi} = (h_{\mathrm{f}}/k_{\mathrm{f}})\sqrt{\Omega/\nu_{\mathrm{f}}}$ is the thermal Biot number.

The surface drag force $C_{f\tilde{r}}$ and heat transfer rate Nu_r are defined as [53, 55]

$$C_{f\tilde{r}} = \frac{1}{\rho_{\mathrm{f}}\tilde{r}^2\Omega^2}\sqrt{\tau_{\tilde{r}}^2 + \tau_{\phi}^2}, \mathrm{Nu}_{\tilde{r}} = \frac{\tilde{r}q_w}{k_{\mathrm{f}}(T_{\mathrm{f}} - T_w)}, \tag{8}$$

where $\tau_{\tilde{r}}$, τ_{ϕ}, and q_w are defined as

$$\tau_r = \mu_{\mathrm{nf}}\left(\frac{\partial\tilde{u}_1}{\partial\tilde{z}} + \frac{\partial\tilde{u}_3}{\partial\tilde{r}}\right)\Bigg|_{\tilde{z}=0},$$

$$\tau_{\phi} = \mu_{\mathrm{nf}}\left(\frac{\partial\tilde{u}_2}{\partial\tilde{z}} + \frac{1}{\tilde{r}}\frac{\partial\tilde{u}_3}{\partial\phi}\right)\Bigg|_{\tilde{z}=0},$$

$$q_w = -k_{\mathrm{nf}}\frac{\partial\tilde{T}}{\partial\tilde{z}}\Bigg|_{\tilde{z}=0}. \tag{9}$$

The dimensionless form of Equation (7) is:

$$\sqrt{\mathrm{Re}}C_{f\tilde{r}} = \bar{M}_1\sqrt{f'^2(0) + g'^2(0)}, \frac{\mathrm{Nu}_r}{\sqrt{\mathrm{Re}}} = -\bar{M}_4\theta'(0), \tag{10}$$

where $\mathrm{Re} = \Omega\tilde{r}^2/\nu_{\mathrm{f}}$ is the local Reynolds number.

3. HAM Solution

The initial guesses and linear operators are defined as

$$f_0(\eta) = 0, g_0(\eta) = \frac{1}{1+\alpha}e^{-\eta}, \theta_0(\eta) = \frac{k_{\mathrm{f}}}{k_{\mathrm{nf}}}\frac{\mathrm{Bi}}{1+\mathrm{Bi}}e^{-\eta},$$

$$L_f = f'' - f, L_g = g'' - g, L_\theta = \theta'' - \theta, \tag{11}$$

with the following properties:

$$L_f[c_1e^{-\eta} + c_2e^{\eta}] = 0, L_g[c_3e^{-\eta} + c_4e^{\eta}] = 0, L_\theta[c_5e^{-\eta} + c_6e^{\eta}] = 0, \tag{12}$$
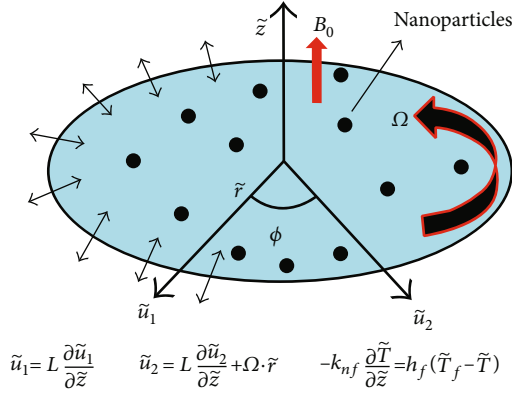
where $c_i(i = 1 - 6)$ are called arbitrary constants.

$$\tilde{u}_1 = L\frac{\partial \tilde{u}_1}{\partial \tilde{z}} \qquad \tilde{u}_2 = L\frac{\partial \tilde{u}_2}{\partial \tilde{z}} + \Omega \cdot \tilde{r} \qquad -k_{nf}\frac{\partial \tilde{T}}{\partial \tilde{z}} = h_f(\tilde{T}_f - \tilde{T})$$

Figure 1: Geometrical representation of the flow problem.

Figure 2: $\hbar$-curves for $f'(0)$, $g'(0)$, and $\theta'(0)$.

4. HAM Convergence

Figure 2 is displayed for the convergence of series solutions. The auxiliary parameters $\hbar_f$, $\hbar_g$, and $\hbar_\theta$ are responsible for the adjustment and controlling of the series solutions. Therefore, the acceptable values for velocities and thermal profiles are $-2.1 \le \hbar_f \le -0.1$, $-1.9 \le \hbar_g \le 0.0$, and $-2.5 \le \hbar_\theta \le 0.2$.

5. Results and Discussion

This segment compacts with the impressions of different embedded factors on velocities and temperature, surface drag force and heat transfer rate. We have considered the spherical-shaped three different nanoparticles like Cu, Al_2O_3, and TiO_2 with a base fluid H_2O. Since water is used as a base fluid, therefore, Pr = 6.2. The thermophysical properties of Cu, Al_2O_3, TiO_2, and H_2O are presented in Table 1. The shape factor and sphericity of the different nanoparticles are presented in Table 2. In Table 3, we have presented the numerical values of skin friction via magnetic parameter for different water-based spherical-shaped nanoparticles and pure water. Both slip and no-slip conditions are considered here. The greater magnetic parameter augments the skin friction coefficient. Actually, the magnetic parameter drops off the velocity function due to Lorentz force. The heightening Lorentz force means the skin friction coefficient augments which has been seen for the spherical-shaped Cu, Al_2O_3, and TiO_2 nanoparticles and pure water for the case of no-slip condition. For the case of slip condition, interesting results have been introduced here. Physically, the presence of slip parameter reduces the velocity of the fluid due augmenting skin friction coefficient as occurs which allow more fluid to past the disk as found for pure water. However, for the spherical-shaped Cu, Al_2O_3, and TiO_2 nanoparticles, the presence of slip and magnetic parameters have diverse impact on surface drag force. In addition, the greater impact of magnetic parameter occurs in the absence of slip effect. Table 4 shows the numerical values of surface drag force via spherical-shaped nanoparticle volume fraction for the different water-based nanoparticles. Physically, the increasing nanoparticle volume fraction means that the nanoparti-
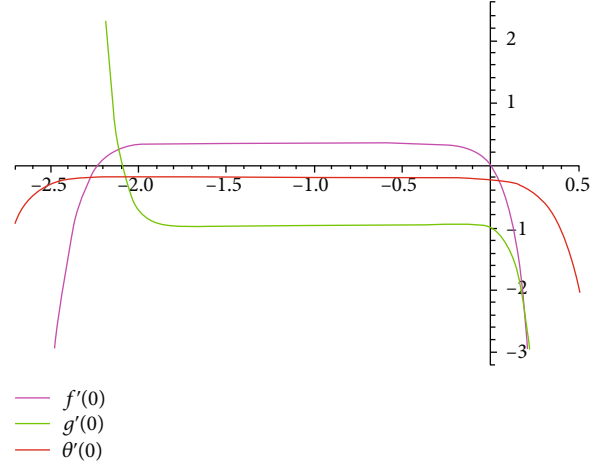
Table 1: Numerical values of the thermophysical properties of H_2O, Cu, Al_2O_3, and TiO_2 [13, 51, 52].

Base fluid and nanoparticles	ρ (kg/m^3)	c_p (J/kgK)	k (W/mK)	σ (1/Ωm)
H_2O	997.1	4179	0.613	0.05
Al_2O_3	3970	765	40	1×10^{-10}
Cu	8933	385	401	5.96×10^7
TiO_2	4250	685.2	8.9539	2.6×10^6

Table 2: Shape factor and sphericity of different particle shapes [56, 57].

Shape of the nanoparticle	Sphericity	Shape factor
Sphere	1.0	3.00
Cylinder	0.62	4.84
Blade	0.36	8.33
Platelet	0.52	5.77
Brick	0.81	3.70

cles and the base fluid collide with each other which accelerates the fluid motion; consequently, the momentum boundary layer thickness decreases and upsurges the surface drag force. Also, the impact of spherical-shaped nanoparticles volume fraction is the same for the local Nusselt number as portrayed in Table 5. Additionally, the surface drag force is greater for the case of no-slip condition. The increasing thermal Biot number augments the heat transfer rate. Tables 6–8 show the comparison of analytical and numerical techniques for $f(\eta)$, $g(\eta)$, and $\theta(\eta)$. Here, a close agreement between both techniques is found. Figure 3 shows the impact of nanoparticle volume fraction on spherical-shaped Cu, Al_2O_3, and TiO_2 nanoparticles. Figure 4 shows the variation in radial velocity of the spherical-shaped Cu, Al_2O_3, and TiO_2 nanoparticles and pure water (H_2O) via a magnetic parameter for the case of no-slip condition. The greater magnetic factor diminishes the radial velocity of the spherical-shaped Cu, Al_2O_3, and TiO_2 nanoparticles and

Table 3: Numerical values of the skin friction via magnetic parameter for different water-based spherical-shaped nanoparticles and pure water.

Magnetic parameter	Values	No-slip condition	Cu	Al_2O_3	TiO_2	Pure water
	1.0		0.97455	0.95901	0.97484	0.94904
	2.0	$\alpha = 0.0$	1.33931	1.30845	1.34076	1.30432
	3.0		1.70971	1.66292	1.71184	1.66454
M		Slip condition				
	1.0		0.69813	0.69369	0.69740	0.82172
	2.0	$\alpha = 0.5$	0.78174	0.77365	0.78104	0.57823
	3.0		0.86542	0.85368	0.86475	0.33615

Table 4: Numerical values of the skin friction via spherical-shaped nanoparticle volume fraction for different water-based nanoparticles.

Nanoparticles volume fraction	Values	No-slip condition	Cu	Al_2O_3	TiO_2
	0.1		0.97455	0.95901	0.97484
	0.2	$\alpha = 0.0$	1.00105	0.96960	1.00142
	0.3		1.02854	0.98086	1.02879
φ		Slip condition			
	0.1		0.69813	0.69369	0.69740
	0.2	$\alpha = 0.5$	0.71727	0.70832	0.71578
	0.3		0.73702	0.72352	0.73397

Table 5: Numerical values of the local Nusselt number via the Biot number and spherical-shaped nanoparticle volume fraction for different water-based nanoparticles and pure water.

Parameters	Values	Cu	Al_2O_3	TiO_2	Pure water
	0.1	0.08433	0.08449	0.08504	0.08787
Bi	0.2	0.15021	0.15050	0.15146	0.15648
	0.3	0.20882	0.20321	0.20450	0.21124
	0.1	0.16124	0.15782	0.14667	—
φ	0.2	0.29520	0.28292	0.24451	—
	0.3	0.54998	0.51512	0.41199	—

Table 6: Analytical and numerical solutions for $f(\eta)$.

η	HAM	Shooting	Absolute error
0.0	1.277200×10^{-17}	0.048458	0.048458
0.5	0.079926	0.157846	0.077921
1.0	0.092998	0.199663	0.106666
1.5	0.083715	0.203372	0.119657
2.0	0.068544	0.186409	0.117866
2.5	0.053523	0.159724	0.106202
3.0	0.040535	0.129866	0.089330
3.5	0.029738	0.100012	0.070274
4.0	0.020472	0.070470	0.049998
4.5	0.011394	0.038415	0.027021
5.0	8.673620×10^{-19}	-0.004014	0.004014

pure water (H_2O). Physically, the applied magnetic field creates Lorentz force during the fluid flow which opposes the motion of the flow nanoparticles; consequently, a reducing impact is observed. For the case of slip condition, a similar impact of magnetic parameter is observed for radial velocity of the spherical-shaped Cu, Al_2O_3, and TiO_2 nanoparticles and pure water (H_2O) as displayed in Figure 5. Furthermore, the presence of a slip parameter reduces the velocity of the fluid due to augmenting skin friction coefficient occuring which allows more fluid to past the disk. So, the combination of magnetic and slip parameters has greater impact on velocity profile of the spherical-shaped Cu, Al_2O_3, and TiO_2 nanoparticles and pure water (H_2O) as compared to no-slip condition. Figure 6 displays the variation in radial velocity $f(\eta)$ of the spherical-shaped Cu, Al_2O_3, and TiO_2 nanoparticles via φ for the case of no-slip condition. The greater φ augments the radial velocity of the spherical-shaped Cu nanoparticle, while it reduces the radial velocity of the spherical-shaped Al_2O_3 and TiO_2 nanoparticles. Physically, the greater φ opposes the motion of the spherical-shaped Al_2O_3 and TiO_2 nanoparticles which augments the boundary layer thickness and slows down the velocity profile, while this impact is opposite for Cu nanoparticle. For the case of slip condition, the greater φ augments the radial velocity of the spherical-shaped Cu nanoparticle, while it reduces the velocity profile for Al_2O_3 and TiO_2 nanoparticles next to the surface of the rotating disk and moderates the increasing effect as $\eta \longrightarrow \infty$ (see Figure 7). Figures 8 and 9 portray the variation in $g(\eta)$ of the spherical-shaped Cu, Al_2O_3, and TiO_2 nanoparticles via a magnetic parameter for the case of no-slip and slip conditions, respectively. For both no-

TABLE 7: Analytical and numerical solutions for $g(\eta)$.

η	HAM	Shooting	Absolute error
0.0	1.000000	0.918880	0.081120
0.5	0.622565	0.730215	0.107650
1.0	0.401548	0.588991	0.187443
1.5	0.263876	0.474205	0.210329
2.0	0.175398	0.377681	0.202282
2.5	0.117530	0.296126	0.178596
3.0	0.079169	0.227544	0.148375
3.5	0.053275	0.169557	0.116282
4.0	0.035073	0.118368	0.083296
4.5	0.020845	0.067299	0.046454
5.0	0.006738	0.003395	0.003343

TABLE 8: Analytical and numerical solutions for $\theta(\eta)$.

η	HAM	Shooting	Absolute error
0.0	0.520728	0.514973	0.005755
0.5	0.407258	0.303778	0.103477
1.0	0.316987	0.170961	0.146029
1.5	0.248884	0.098508	0.150376
2.0	0.196218	0.059782	0.136436
2.5	0.153566	0.038072	0.115494
3.0	0.117379	0.024878	0.092501
3.5	0.085413	0.016085	0.069328
4.0	0.056215	0.009652	0.046563
4.5	0.028772	0.004487	0.024285
5.0	0.002246	-0.000105	0.002351
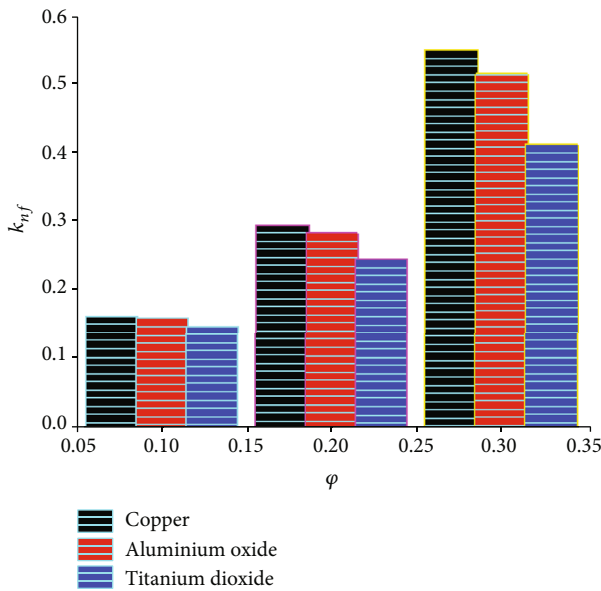
FIGURE 3: Impact of nanoparticle volume fraction on spherical-shaped nanoparticles of water-based Cu, Al_2O_3, and TiO_2.
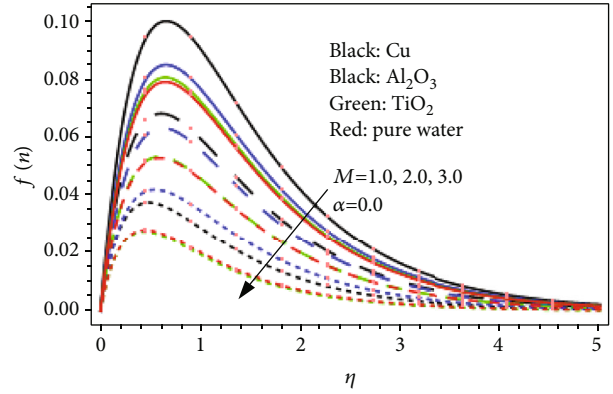
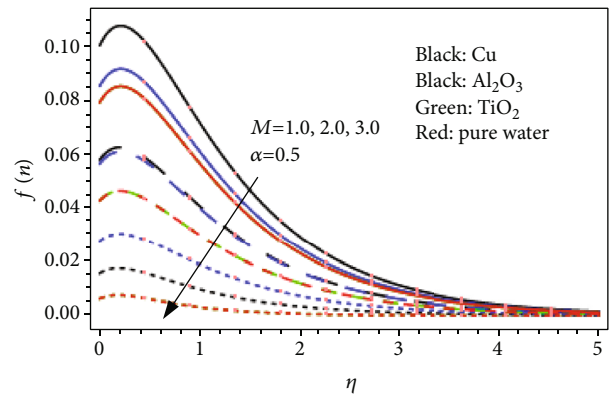FIGURE 4: Variation in $f(\eta)$ via M when $\alpha = 0.0$.

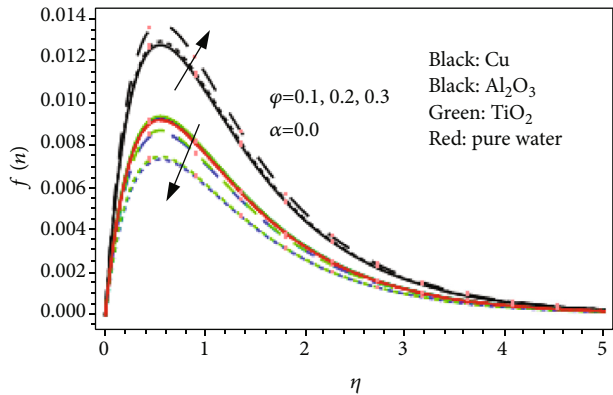FIGURE 5: Variation in $f(\eta)$ via M when $\alpha = 0.5$.

FIGURE 6: Variation in $f(\eta)$ via φ when $\alpha = 0.0$.

slip and slip conditions, similar impacts are found here as seen in Figures 4 and 5. However, the impact of slip condition is greater for $f(\eta)$ as compared to $g(\eta)$. Figure 10 shows the variation in velocity profile $g(\eta)$ of the spherical-shaped Cu, Al_2O_3, and TiO_2 nanoparticles via φ for the case when $\alpha = 0.0$. The greater φ augments the velocity profile $g(\eta)$ of the spherical-shaped Cu, Al_2O_3, and TiO_2 nanoparticles. Physically, the greater φ opposes the motion of the spherical-shaped Cu, Al_2O_3, and TiO_2 nanoparticles which augments the boundary layer thickness and slows down the velocity profile. For the case when $\alpha = 0.5$, the greater
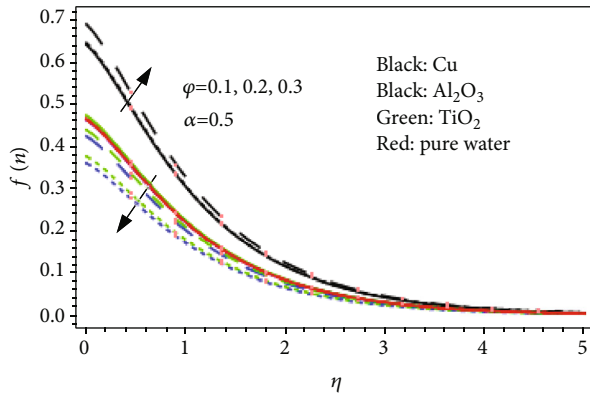
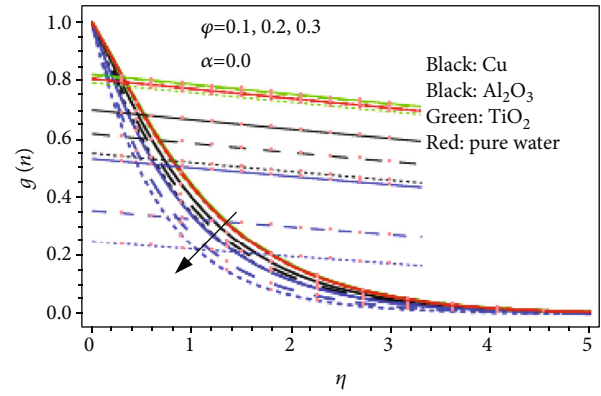FIGURE 7: Variation in $f(\eta)$ via φ when $\alpha = 0.5$.
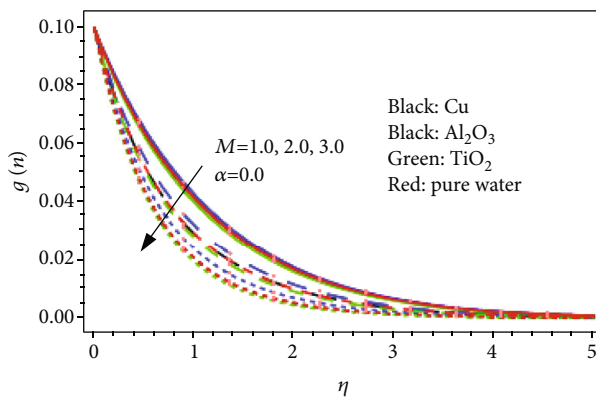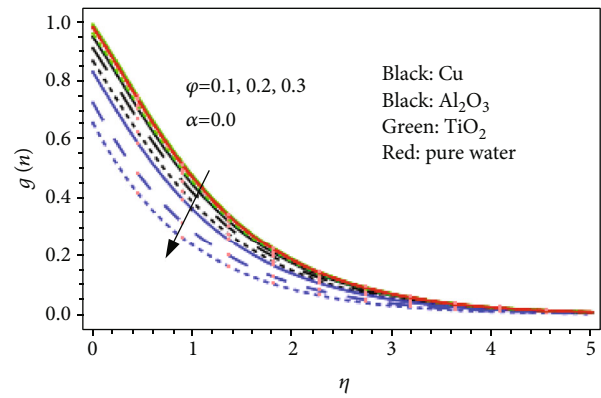

FIGURE 8: Variation in $g(\eta)$ via M when $\alpha = 0.0$.

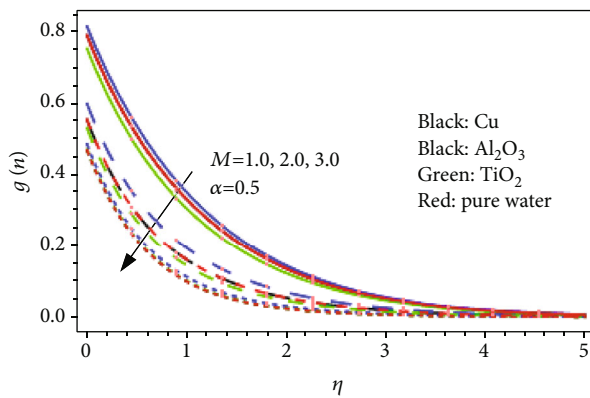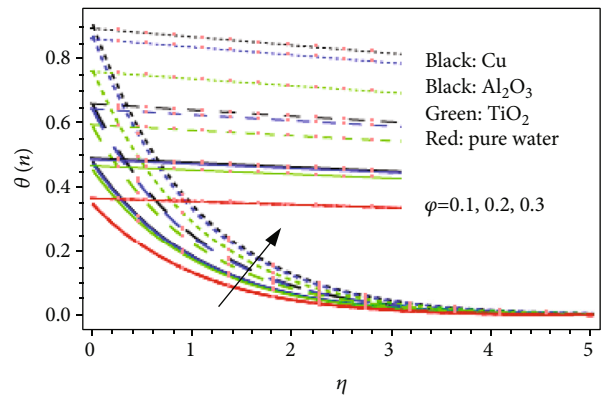FIGURE 9: Variation in $g(\eta)$ via M when $\alpha = 0.5$.

FIGURE 10: Variation in $g(\eta)$ via φ when $\alpha = 0.0$.

FIGURE 11: Variation in $g(\eta)$ via φ when $\alpha = 0.5$.

FIGURE 12: Variation in $\theta(\eta)$ via φ.

φ reduces the velocity profile $g(\eta)$ of the spherical-shaped Cu, Al_2O_3, and TiO_2 nanoparticles (see Figure 11). Additionally, the reducing impact of φ is greater for $\alpha = 0.5$ as compared to $\alpha = 0.0$. Figure 12 shows the variation in temperature profile $\theta(\eta)$ of the spherical-shaped Cu, Al_2O_3, and TiO_2 nanoparticles via φ. The greater φ augments the temperature profile. Physically, the greater φ upsurges the thermal conductivity of the Cu, Al_2O_3, and TiO_2 nanoparticles and thermal transfer rate. Therefore, the nanoparticle which has high thermal conductivity has the dominant impact on temperature profile and heat transfer rate as

shown in Figure 3 and Table 5. Here, Cu nanoparticle has greater thermal conductivity than Al_2O_3 nanoparticle, and Al_2O_3 nanoparticle has greater thermal conductivity than TiO_2 nanoparticle. So, the greatest impact of Cu nanoparticle is found here. Figure 13 shows the variation in temperature profile $\theta(\eta)$ of the spherical-shaped Cu, Al_2O_3, and TiO_2 nanoparticles via the thermal Biot number. The greater Biot number augments the thermal profile $\theta(\eta)$ of the spherical-shaped Cu, Al_2O_3, and TiO_2 nanoparticles. Physically, the heat transfer coefficient caused by the hot fluid is directly related to the Biot number. Therefore, the greater
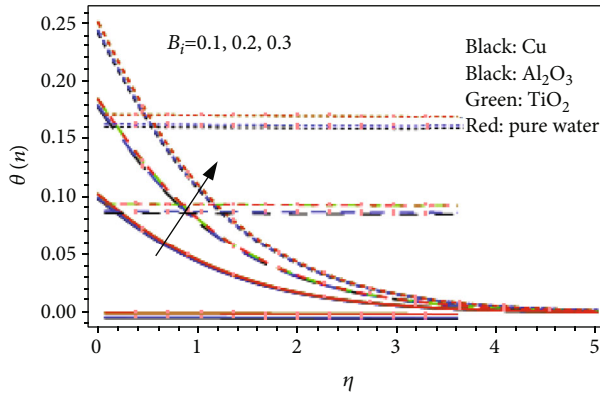
FIGURE 13: Variation in $\theta(\eta)$ via Bi.

Biot number raises the convection and thermal profile significantly. Additionally, the spherical-shaped Cu nanoparticle has greater impact on thermal profile as compared to Al_2O_3 and TiO_2 nanoparticles.

6. Conclusion

In this work, we have examined the water-based spherical-shaped nanoparticles of copper-water, aluminum oxide-water, titanium dioxide-water, and pure water past a rotating disk. Slip and no-slip conditions are considered in order to examine the variations in radial and tangential velocities due to the magnetic field, nanoparticle volume fraction, and thermal Biot number. The final points are mentioned below:

(a) For $\alpha = 0.5$, the surface drag force of Cu, Al_2O_3, and TiO_2 have reduced with the increasing magnetic parameter, while for $\alpha = 0.0$, the surface drag force of the Cu, Al_2O_3, and TiO_2 nanoparticles have augmented with the increasing magnetic parameter. Additionally, the greater impact of magnetic parameter occurs when $\alpha = 0.5$

(b) The surface drag force and heat transfer rate of spherical-shaped nanoparticles of Cu, Al_2O_3, and TiO_2 is augmented via nanoparticle volume fraction

(c) For $\alpha = 0.5$ and $\alpha = 0.0$, the radial and tangential velocities of the spherical-shaped nanoparticles of Cu, Al_2O_3, and TiO_2 and pure water have augmented via a magnetic parameter. Additionally, the impact of magnetic field is greater for radial velocity as compared to tangential velocity

(d) For $\alpha = 0.5$ and $\alpha = 0.0$, the tangential velocity of the spherical-shaped nanoparticle of Cu, Al_2O_3, and TiO_2 has reduced via nanoparticle volume fraction. Additionally, the reducing impact of nanoparticle volume fraction is greater for $\alpha = 0.5$ as compared to $\alpha = 0.0$

(e) The greater nanoparticle volume fraction and thermal Biot number have increased the temperature

profile of the spherical-shaped nanoparticles of Cu, Al_2O_3, and TiO_2

Nomenclature

B_0:	Strength of magnetic field
Bi:	Thermal Biot number
C_f:	Skin friction coefficient
$c_i (i = 1 - 6)$:	Arbitrary constants
c_p:	Heat capacitance
f_0, θ_0, g_0:	Initial guesses
k:	Thermal conductivity
L:	Wall slip parameter
L_f, L_g, L_θ:	Linear operators
M:	Magnetic parameter
Nu:	Nusselt number
$\tilde{p}$:	Pressure
Re:	Reynolds number
Pr:	Prandtl number
$\tilde{r}, \phi, \tilde{z}$:	Coordinates
$\tilde{u}_1, \tilde{u}_2, \tilde{u}_3$:	Velocity components

Greek Letters

Ω:	Angular velocity
σ:	Electrical conductivity
ρ:	Density
μ:	Dynamic viscosity
α:	Dimensionless wall slip parameter
φ:	Volume fraction of the nanoparticles

Subscripts

f:	Fluid
nf:	Nanofluids
np:	Nanoparticles.

Data Availability

All the supporting data are within the manuscript.

Conflicts of Interest

The authors declare that they have no conflict of interest.

References

[1] H. Upreti and M. Kumar, "Influence of non-linear radiation, Joule heating and viscous dissipation on the boundary layer flow of MHD nanofluid flow over a thin moving needle," *Multidiscipline Modeling in Materials and Structures*, vol. 16, no. 1, pp. 208–224, 2020.

[2] J. Raza, F. Mebarek-Oudina, and A. J. Chamkha, "Magnetohydrodynamic flow of molybdenum disulfide nanofluid in a channel with shape effects," *Multidiscipline Modeling in Materials and Structures*, vol. 15, no. 4, pp. 737–757, 2019.

[3] J. Raza, F. Mebarek-Oudina, and B. Mahanthesh, "Magnetohydrodynamic flow of nano Williamson fluid generated by stretching plate with multiple slips," *Multidiscipline Modeling in Materials and Structures*, vol. 15, no. 5, pp. 871–894, 2019.

[4] J. Raza, M. Farooq, F. Mebarek-Oudina, and B. Mahanthesh, "Multiple slip effects on MHD non-Newtonian nanofluid flow over a nonlinear permeable elongated sheet," *Multidiscipline Modeling in Materials and Structures*, vol. 15, no. 5, pp. 913–931, 2019.

[5] C. Sulochana and S. R. Aparna, "Unsteady magnetohydrodynamic radiative liquid thin film flow of hybrid nanofluid with thermophoresis and Brownian motion," *Multidiscipline Modeling in Materials and Structures*, vol. 16, no. 4, pp. 811–834, 2020.

[6] S. S. Giri, K. Das, and P. K. Kundu, "Inclined magnetic field effects on unsteady nanofluid flow and heat transfer in a finite thin film with non-uniform heat source/sink," *Multidiscipline Modeling in Materials and Structures*, vol. 15, no. 1, pp. 265–282, 2019.

[7] A. Kumar, V. Sugunamma, N. Sandeep et al., "Impact of Brownian motion and thermophoresis on bioconvective flow of nanoliquids past a variable thickness surface with slip effects," *Multidiscipline Modeling in Materials and Structures*, vol. 15, no. 1, pp. 103–132, 2019.

[8] A. A. Minea, *Advances in New Heat Transfer Fluids: From Numerical to Experimental Techniques*, CRC Press, 2017.

[9] M. Sheikholeslami, "Numerical approach for MHD Al2O3-water nanofluid transportation inside a permeable medium using innovative computer method," *Computer Methods in Applied Mechanics and Engineering*, vol. 344, pp. 306–318, 2019.

[10] T. Hayat, B. Ahmed, F. M. Abbasi, and A. Alsaedi, "Peristalsis of nanofluid through curved channel with Hall and Ohmic heating effects," *Journal of Central South University*, vol. 26, no. 9, pp. 2543–2553, 2019.

[11] M. Sheikholeslami, "Finite element method for PCM solidification in existence of CuO nanoparticles," *Journal of Molecular Liquids*, vol. 265, pp. 347–355, 2018.

[12] T. Thumma, S. R. Mishra, and O. A. Bég, "ADM solution for Cu/CuO–water viscoplastic nanofluid transient slip flow from a porous stretching sheet with entropy generation, convective wall temperature and radiative effects," *Journal of Applied and Computational Mechanics*, vol. 7, no. 3, pp. 1291–1305, 2021.

[13] T. Hayat, B. Ahmed, F. M. Abbasi, and A. Alsaedi, "Hydromagnetic peristalsis of water based nanofluids with temperature dependent viscosity: a comparative study," *Journal of Molecular Liquids*, vol. 234, pp. 324–329, 2017.

[14] M. Sheikholeslami, M. B. Gerdroodbary, R. Moradi, A. Shafee, and Z. Li, "Application of neural network for estimation of heat transfer treatment of Al_2O_3-H_2O nanofluid through a channel," *Computer Methods in Applied Mechanics and Engineering*, vol. 344, pp. 1–12, 2019.

[15] T. Thumma, O. Anwar Bég, and A. Kadir, "Numerical study of heat source/sink effects on dissipative magnetic nanofluid flow from a non-linear inclined stretching/shrinking sheet," *Journal of Molecular Liquids*, vol. 232, pp. 159–173, 2017.

[16] B. C. Rout, S. R. Mishra, and T. Thumma, "Effect of viscous dissipation on Cu-water and Cu-kerosene nanofluids of axisymmetric radiative squeezing flow," *Heat Transfer—Asian Research*, vol. 48, no. 7, pp. 3039–3054, 2019.

[17] T. Gul, S. Nasir, S. Islam, Z. Shah, and M. A. Khan, "Effective Prandtl number model influences on the γAl_2O_3-H_2O and γAl_2O_3-$C_2H_6O_2$ nanofluids spray along a stretching cylinder," *Arabian Journal for Science and Engineering*, vol. 44, 2019.

[18] T. Gul and K. Firdous, "The experimental study to examine the stable dispersion of the graphene nanoparticles and to look at the GO–H_2O nanofluid flow between two rotating disks," *Applied Nanoscience*, vol. 8, no. 7, pp. 1711–1727, 2018.

[19] H. Štorkánová, S. Oreská, M. Špiritović et al., "Plasma Hsp90 levels in patients with systemic sclerosis and relation to lung and skin involvement: a cross-sectional and longitudinal study," *Scientific Reports*, vol. 11, no. 1, pp. 1–15, 2021.

[20] W. Alghamdi, A. Alsubie, P. Kumam, A. Saeed, and T. Gul, "MHD hybrid nanofluid flow comprising the medication through a blood artery," *Scientific Reports*, vol. 11, no. 1, pp. 1–13, 2021.

[21] Z. Boulahia, A. Wakif, and R. Sehaqui, "Finite volume analysis of free convection heat transfer in a square enclosure filled by a Cu-water nanofluid containing different shapes of heating cylinder," *Journal of Nanofluids*, vol. 6, no. 4, pp. 761–768, 2017.

[22] Z. Boulahia, A. Wakif, and R. Sehaqui, "Numerical modeling of natural convection heat transfer in a wavy wall enclosure filled by a Cu-water nanofluid with a square cooler," *Journal of Nanofluids*, vol. 6, no. 2, pp. 324–333, 2017.

[23] A. Shafiq, G. Rasool, H. Alotaibi et al., "Thermally enhanced Darcy-Forchheimer Casson-water/glycerine rotating nanofluid flow with uniform magnetic field," *Micromachines*, vol. 12, no. 6, p. 605, 2021.

[24] A. Wakif, Z. Boulahia, S. R. Mishra, M. Mehdi Rashidi, and R. Sehaqui, "Influence of a uniform transverse magnetic field on the thermo-hydrodynamic stability in water-based nanofluids with metallic nanoparticles using the generalized Buongiorno's mathematical model," *The European Physical Journal Plus*, vol. 133, no. 5, p. 181, 2018.

[25] Z. Boulahia, A. Wakif, A. J. Chamkha, and R. Sehaqui, "Numerical study of natural and mixed convection in a square cavity filled by a Cu–water nanofluid with circular heating and cooling cylinders," *Mechanics & Industry*, vol. 18, no. 5, p. 502, 2017.

[26] A. Dawar, Z. Shah, W. Khan, M. Idrees, and S. Islam, "Unsteady squeezing flow of magnetohydrodynamic carbon nanotube nanofluid in rotating channels with entropy generation and viscous dissipation," *Advances in Mechanical Engineering*, vol. 11, no. 1, Article ID 1687814018823310, 2019.

[27] H. Tamim, S. Dinarvand, R. Hosseini, and I. Pop, "MHD mixed convection stagnation-point flow of a nanofluid over a vertical permeable surface: a comprehensive report of dual solutions," *Heat and Mass Transfer*, vol. 50, no. 5, pp. 639–650, 2014.

[28] S. S. Ghadikolaei, M. Yassari, H. Sadeghi, K. Hosseinzadeh, and D. D. Ganji, "Investigation on thermophysical properties of Tio_2-Cu/H_2O hybrid nanofluid transport dependent on shape factor in MHD stagnation point flow," *Powder Technology*, vol. 322, pp. 428–438, 2017.

[29] T. Hayat, S. Qayyum, M. Imtiaz, and A. Alsaedi, "MHD flow and heat transfer between coaxial rotating stretchable disks in a thermally stratified medium," *PLoS One*, vol. 11, no. 5, article e0155899, 2016.

[30] R. Ahmad, M. Mustafa, T. Hayat, and A. Alsaedi, "Numerical study of MHD nanofluid flow and heat transfer past a bidirectional exponentially stretching sheet," *Journal of Magnetism and Magnetic Materials*, vol. 407, pp. 69–74, 2016.

[31] P. Singh, A. K. Pandey, and M. Kumar, "Forced convection in MHD slip flow of alumina-water nanofluid over a flat plate," *Journal of Enhanced Heat Transfer*, vol. 23, no. 6, pp. 487–497, 2016.

[32] B. Mliki, M. A. Abbassi, A. Omri, and B. Zeghmati, "Effects of nanoparticles Brownian motion in a linearly/sinusoidally heated cavity with MHD natural convection in the presence of uniform heat generation/absorption," *Powder Technology*, vol. 295, pp. 69–83, 2016.

[33] H. Upreti, A. K. Pandey, M. Kumar, and O. D. Makinde, "Ohmic heating and non-uniform heat source/sink roles on 3D Darcy–Forchheimer flow of CNTs nanofluids over a stretching surface," *Arabian Journal for Science and Engineering*, vol. 45, no. 9, pp. 7705–7717, 2020.

[34] A. K. Pandey and M. Kumar, "MHD flow inside a stretching/shrinking convergent/divergent channel with heat generation/absorption and viscous-ohmic dissipation utilizing CU-WATER nanofluid," *Computational Thermal Sciences: An International Journal*, vol. 10, no. 5, pp. 457–471, 2018.

[35] M. Turkyilmazoglu, "Nanofluid flow and heat transfer due to a rotating disk," *Computers and Fluids*, vol. 94, pp. 139–146, 2014.

[36] A. Hussain, S. T. Mohyud-Din, and T. A. Cheema, "Analytical and numerical approaches to squeezing flow and heat transfer between two parallel disks with velocity slip and temperature jump," *Chinese Physics Letters*, vol. 29, no. 11, article 114705, 2012.

[37] N. A. Alreshidi, Z. Shah, A. Dawar, P. Kumam, M. Shutaywi, and W. Watthayu, "Brownian motion and thermophoresis effects on MHD three dimensional nanofluid flow with slip conditions and joule dissipation due to porous rotating disk," *Molecules*, vol. 25, no. 3, p. 729, 2020.

[38] A. Dawar, Z. Shah, P. Kumam et al., "Chemically reactive MHD micropolar nanofluid flow with velocity slips and variable heat source/sink," *Scientific Reports*, vol. 10, no. 1, pp. 1–23, 2020.

[39] M. W. Ahmad, P. Kumam, Z. Shah et al., "Darcy-Forchheimer MHD couple stress 3D nanofluid over an exponentially stretching sheet through Cattaneo-Christov convective heat flux with zero nanoparticles mass flux conditions," *Entropy*, vol. 21, no. 9, p. 867, 2019.

[40] I. Waini, A. Ishak, and I. Pop, "MHD flow and heat transfer of a hybrid nanofluid past a permeable stretching/shrinking wedge," *Applied Mathematics and Mechanics*, vol. 41, no. 3, pp. 507–520, 2020.

[41] K. Vajravelu, K. V. Prasad, C.-O. Ng, and H. Vaidya, "MHD squeeze flow and heat transfer of a nanofluid between parallel disks with variable fluid properties and transpiration," *International Journal of Mechanical and Materials Engineering*, vol. 12, no. 1, pp. 1–14, 2017.

[42] T. Gul, R. A. Shah, S. Islam, and M. Arif, "MHD thin film flows of a third grade fluid on a vertical belt with slip boundary conditions," *Journal of Applied Mathematics*, vol. 2013, Article ID 707286, 14 pages, 2013.

[43] A. S. Alshomrani and T. Gul, "A convective study of Al_2O_3-H_2O and Cu- H_2O nano-liquid films sprayed over a stretching cylinder with viscous dissipation," *International Journal of Mechanical and Materials Engineering*, vol. 132, no. 11, pp. 1–16, 2017.

[44] T. Gul, Kashifullah, M. Bilal, W. Alghamdi, M. I. Asjad, and T. Abdeljawad, "Hybrid nanofluid flow within the conical gap between the cone and the surface of a rotating disk," *Scientific Reports*, vol. 11, no. 1, p. 1180, 2021.

[45] T. Gul, H. Anwar, M. A. Khan, I. Khan, and P. Kumam, "Integer and non-integer order study of the GO-W/GO-EG nano-

[46] G. Reiss and A. Hütten, "Applications beyond data storage," *Nature Materials*, vol. 4, no. 10, pp. 725-726, 2005.

[47] D. Faivre and M. Bennet, "Magnetic nanoparticles line up," *Nature*, vol. 535, no. 7611, pp. 235-236, 2016.

[48] G. Priyadarshana, N. Kottegoda, A. Senaratne, A. De Alwis, and V. Karunaratne, "Synthesis of magnetite nanoparticles by top-down approach from a high purity ore," *Journal of Nanomaterials*, vol. 2015, 8 pages, 2015.

[49] Y. Zhou, C.-K. Dong, L. L. Han, J. Yang, and X. W. du, "Top-down preparation of active cobalt oxide catalyst," *ACS Catalysis*, vol. 6, no. 10, pp. 6699–6703, 2016.

[50] U. Rashid, D. Baleanu, A. Iqbal, and M. Abbas, "Shape effect of nanosize particles on magnetohydrodynamic nanofluid flow and heat transfer over a stretching sheet with entropy generation," *Entropy*, vol. 22, no. 10, p. 1171, 2020.

[51] H. F. Oztop and E. Abu-Nada, "Numerical study of natural convection in partially heated rectangular enclosures filled with nanofluids," *International Journal of Heat and Fluid Flow*, vol. 29, no. 5, pp. 1326–1336, 2008.

[52] M. Sheikholeslami, M. Gorji-Bandpy, and D. D. Ganji, "Numerical investigation of MHD effects on Al2O3–water nanofluid flow and heat transfer in a semi-annulus enclosure using LBM," *Energy*, vol. 60, pp. 501–510, 2013.

[53] P. Ragupathi, T. Muhammad, S. Islam, and A. Wakif, "Application of Arrhenius kinetics on MHD radiative Von Kármán Casson nanofluid flow occurring in a Darcy-Forchheimer porous medium in the presence of an adjustable heat source," *Physica Scripta*, vol. 96, article 125228, 2021.

[54] T. V. Kármán, "Über laminare und turbulente Reibung," *ZAMM-Journal of Applied Mathematics and Mechanics/Zeitschrift für Angewandte Mathematik und Mechanik*, vol. 1, pp. 233–252, 1921.

[55] U. Khan, S. Bilal, A. Zaib, O. D. Makinde, and A. Wakif, "Numerical simulation of a nonlinear coupled differential system describing a convective flow of Casson gold–blood nanofluid through a stretched rotating rigid disk in the presence of Lorentz forces and nonlinear thermal radiation," *Numerical Methods for Partial Differential Equations*, 2020.

[56] R. L. Hamilton and O. K. Crosser, "Thermal conductivity of heterogeneous two-component systems," *Industrial and Engineering Chemistry Fundamentals*, vol. 1, no. 3, pp. 187–191, 1962.

[57] E. V. Timofeeva, J. L. Routbort, and D. Singh, "Particle shape effects on thermophysical properties of alumina nanofluids," *Journal of Applied Physics*, vol. 106, no. 1, article 14304, 2009.